Estimation of longitudinal resolution in optical coherence imaging

Ceyhun Akcay, Pascale Parrein, and Jannick P. Rolland

The spectral shape of a source is of prime importance in optical coherence imaging because it determines several aspects of image quality, especially longitudinal resolution. Wide spectral bandwidth, which provides short coherence length, is sought to obtain high-resolution imaging. To estimate longitudinal resolution, the spectral shape of a source is usually assumed to be Gaussian, although the spectra of real sources are typically non-Gaussian. We discuss the limit of this assumption regarding the estimation of longitudinal resolution. To this end, we also investigate how coherence length is related to longitudinal resolution through the evaluation of different definitions of the coherence length. To demonstrate our purpose, the coherence length for several theoretical and real spectral shapes of sources having the same spectral bandwidth and central wavelength is computed. The reliability of coherence length computations toward the estimation of longitudinal resolution is discussed. © 2002 Optical Society of America

OCIS codes: 030.1640, 110.4500, 350.5730.

1. Introduction

Optical coherence imaging is a biomedical imaging technique based on low-coherence interferometry, which operates on the basic principle that two broadband fields interfere only if the optical path difference of the interferometer arms is within the coherence length of the source.[1–5] Thus the coherence length sets the temporal width of the interferometric signal formed by the low-coherence interferometer and consequently sets an upper bound on the longitudinal resolution of the imaging system. The impact of noise in optical coherence imaging is voluntarily disregarded in the present investigation, given that noise will decrease longitudinal resolution. We focus here on the choice of the source to estimate an upper bound on resolution.

The power spectral density (PSD) of the source, which is fully characterized by its shape, its spectral bandwidth, and its center wavelength, is at the base of coherence length computing and has a critical importance for the ability to resolve small structures in optical coherence imaging such as optical coherence tomography[1] and optical coherence microscopy.[4] In this paper we investigate optical coherence imaging cases in which the self-coherence function is the determining factor of longitudinal resolution. The impact on longitudinal resolution of high-numerical-aperture focusing of light in the sample, when it has to be taken into account, is discussed in detail in the literature.[3]

In coherence imaging, the coherence length appears in the detected signal through the self-coherence function, which can be regarded as the point-spread function (PSF) of the imaging system.[6] There are various metrics for the measurement of coherence length from the self-coherence function: full width at half-maximum (FWHM), the width at e^{-1} of the maximum, and the equivalent width.[7] The coherence length has also been defined as the product of the speed of light c with the coherence time τ_c computed from the normalized self-coherence function as reviewed in Subsection 2.A.

In this paper we first review two common metrics for computing the coherence length. We then define the longitudinal resolution and its relation to the coherence length of a source in optical coherence imaging. Theoretical results of computed coherence lengths for two theoretical PSDs, the Gaussian and the Lorentzian, and a real PSD of a superluminescent diode (SLD), all centered at 950 nm and having a 62-nm bandwidth, are then presented. Importantly

The authors are with the School of Optics, Center for Research and Education in Optics and Lasers, University of Central Florida, P.O. Box 162700, 4000 Central Florida Boulevard, Orlando, Florida 32816-2700. J. P. Rolland's e-mail address is jannick@odalab.ucf.edu.

for practical trends in coherence imaging, we finally present a theoretical estimation of coherence length for sources of extended spectral bandwidths, yet with bumpy spectral profiles, and discuss the validity of the relationship between coherence length and longitudinal resolution.

2. Computing Coherence Length and Defining Resolution in Coherence Imaging

After reviewing two common definitions of coherence length, we model the detected signal issued from two layers and evaluate whether either one of these formulas can be used consistently to predict resolution.

A. Computing Coherence Length

The coherence length defined as the FWHM of the self-coherence function has been used most extensively to predict the longitudinal resolution in optical coherence imaging. Several groups have carried out experimental assessments showing a good agreement between the self-coherence width predicted from the source spectrum and the measured PSF.[8–10] The two last examples (Refs. 9 and 10), which employ, respectively, a SLD and a Ti:Al$_2$O$_3$ laser, underline the need to take into account the fact that their sources were not Gaussian to evaluate the coherence length.

An interferometric signal is the correlation between the fields issued from the reference arm $E_R(\mathbf{r}, z_R)$ and the sample arm $E_S(\mathbf{r}, z_S)$ of the interferometer, where $\mathbf{r}$ is the transverse position at the detector, and z_R and z_S are the optical path length in the reference and sample arms, respectively. The optical path-length difference $\Delta z = (z_S - z_R)$ between both of the arms can be translated into a temporal term $\tau = 2\,\Delta z/c$. The interferometric signal $I(\tau)$ given by

$$I(\tau) \propto \mathrm{Re}\left\langle \int_A E_R(\mathbf{r},\, t + \tau)\, E_S{}^*(\mathbf{r},\, t)\mathrm{d}\mathbf{r} \right\rangle, \qquad (1)$$

where the spatial integration is over the detector area $\mathbf{A}$ and the angle brackets correspond to the temporal integration over the detection time that is greater than the coherence time of the source. When the fields in both arms are the same, the right-hand term in relation 1 simply represents the autocorrelation of the fields.

The PSD of a signal is the Fourier transform of its autocorrelation function, also called the self-coherence function, as stated by the Wiener–Khintchine theorem.[11] The inverse Fourier transform of a PSD $S(\lambda)$, where λ is the wavelength, is the self-coherence function $\Gamma(\tau)$ {i.e., $\Gamma(\tau) = \mathscr{F}^{-1}[S(\lambda)]$}, where τ denotes the time delay. The complex temporal coherence function (or complex degree of temporal coherence function) $\gamma(\tau)$ is defined as the normalized self-coherence function and given by $\Gamma(\tau)/\Gamma(0)$.

A first, most commonly employed metric for the coherence length is the FWHM of the modulus of the complex temporal coherence function $|\gamma(\tau)|$:

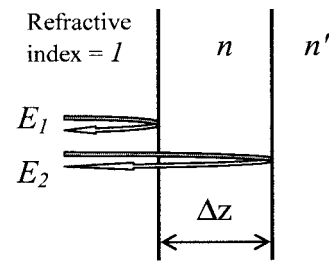$$l_{c_{\mathrm{FWHM}}} = c(\tau' - \tau'') = c\tau_{\mathrm{FWHM}}, \qquad (2)$$

Fig. 1. Two-layer model to determine the longitudinal resolution.

where $|\gamma(\tau')| = |\gamma(\tau'')| = |\gamma(0)|/2$.

Another metric for the coherence length is that defined as the product of the speed of light c and the coherence time τ_c given by[6,12]

$$l_c = c \int_{-\infty}^{\infty} |\gamma(\tau)|^2 \mathrm{d}\tau. \qquad (3)$$

B. Coherence Length and Resolution

A general definition of longitudinal resolution accepted in optical coherence imaging is half of the coherence length of the source (i.e., $l_{c_{\mathrm{FWHM}}}/2$ or $l_c/2$).[3,13] The choice of the FWHM of $|\gamma(\tau)|$ for coherence length, most commonly chosen as mentioned above, is historical in nature and derived from the Rayleigh resolution criterion, which states that two equally bright point sources are barely resolved when the first zero of the Airy disk of the image of one point (which is the PSF of the imaging system for a circular aperture) is at the center of the Airy disk of the image of the other point. In this configuration, the resulting image intensity at the center corresponds to 73.5% of the intensity at the peaks.[6] It is important to note that the shape of the PSF is critical to the value of the composed image intensity at the center, as we show in this paper. Therefore a criterion for Airy-disk-shaped PSFs may not necessarily apply generally to other shaped functions.

If we return to fundamentals, the longitudinal resolution of an optical coherence imaging system is the minimum longitudinal separation detectable in two successive distinct locations (or layers) in the sample with different optical characteristics, where backreflections occur. If we denote Δz the minimal distance between two layers that can be detected, E_1 the field reflected from the first layer at position z_S, E_2 the field reflected from the second layer at position $z_S + \Delta z$, and n the average index of refraction separating the layers as shown in Fig. 1, the interferometric signal becomes

$$I(\tau) \propto \mathrm{Re}\left\langle \int_A E_R(\mathbf{r},\, t + \tau)\, E_1{}^*(\mathbf{r},\, t)\mathrm{d}\mathbf{r} \right\rangle$$
$$+ \mathrm{Re}\left\langle \int_A E_R(\mathbf{r},\, t + \tau)\, E_2{}^*\left(\mathbf{r},\, t - \frac{2n\Delta z}{c}\right)\mathrm{d}\mathbf{r} \right\rangle. \qquad (4)$$

Thus

$$I(\tau) \propto \text{Re}[\gamma(\tau)] + \alpha \, \text{Re}\left[\gamma\left(\tau - \frac{2n\Delta z}{c}\right)\right]. \quad (5)$$

In establishing an upper bound for longitudinal resolution, we assume that the displacement between two layers Δz is an integer multiple of the center wavelength of the source in the material of propagation. Hence the temporal coherence functions are assumed to be in phase. In this case, the envelope of the detected signal is proportional to the summation of the modulus of the two temporal coherence functions with a time delay in between them. If a phase mismatch exists, the resulting signal will also depend on the phase of the complex temporal coherence functions. The assumption of phase matching leads to the worst result in terms of resolution. However, we use this assumption to be able to compare the metrics. Experimental assessments may reveal enhanced resolution that could be predicted on the basis of the subsampling of Δz.

3. Simulation Results

The different light sources are defined in Subsections 3.A and 3.B where we present computational results of coherence length for the PSD of a real source and equivalent (i.e., same bandwidth and central wavelength) Gaussian and Lorentzian PSDs. We further investigate how spectral dips in a Gaussian PSD affect coherence length. To obtain further insight into the relationship between resolution and coherence length, in Subsection 3.C we present simulations demonstrating the ability of different light sources with the specified PSDs of Subsections 3.A and 3.B to resolve the location of two layers.

A. Coherence Length Computation of a Real Source and Equivalent Power Spectral Densities

Light sources employed in optical coherence imaging systems usually have PSDs $S(\lambda)$ approximated to a Gaussian function to estimate resolution.[3,4,9,10,14] A general expression for a normalized Gaussian PSD [i.e., $\int S(\lambda)d\lambda = 1$] and its inverse Fourier transform $\Gamma(\tau)$ is given by

$$S(\lambda) = \frac{2\sqrt{\ln 2}\,\lambda_0^{\,2}}{\sqrt{\pi}c\Delta\lambda} \exp\left\{-\left[2\sqrt{\ln 2}\,\frac{\left(\frac{1}{\lambda} - \frac{1}{\lambda_0}\right)}{\left(\frac{\Delta\lambda}{\lambda_0^{\,2}}\right)}\right]^2\right\}, \quad (6)$$

$$\Gamma(\tau) = \exp\left[-\left(\frac{\pi c \Delta\lambda \tau}{\lambda_0^{\,2}\, 2\sqrt{\ln 2}}\right)^2\right]\exp\left[-j\left(\frac{2\pi c\tau}{\lambda_0}\right)\right], \quad (7)$$

where λ_0 is the center wavelength and $\Delta\lambda$ is the -3-dB spectral bandwidth. $\Gamma(\tau)$ is by definition normalized to one. For the normalized Gaussian PSD,

the coherence lengths computed with the two metrics given by Eqs. (2) and (3), respectively, are

$$l_{c_{\text{FWHM}}} = \frac{4\ln 2}{\pi}\frac{\lambda_0^{\,2}}{\Delta\lambda}, \quad (8)$$

$$l_c = \sqrt{\frac{2\ln 2}{\pi}}\frac{\lambda_0^{\,2}}{\Delta\lambda}. \quad (9)$$

If the PSD of the source is Lorentzian instead of Gaussian, $S(\lambda)$ and $\Gamma(\tau)$ are given by

$$S_{lzn}(\lambda) = 2\left(\left(\pi c\frac{\Delta\lambda}{\lambda_0^{\,2}}\right)\left\{1 + \left[2\frac{\left(\frac{1}{\lambda} - \frac{1}{\lambda_0}\right)}{\frac{\Delta\lambda}{\lambda_0^{\,2}}}\right]^2\right\}\right)^{-1}, \quad (10)$$

$$\Gamma_{lzn}(\tau) = \exp\left(-\frac{\pi c\Delta\lambda}{\lambda_0^{\,2}}|\tau|\right)\exp\left[-j\left(\frac{2\pi c\tau}{\lambda_0}\right)\right]. \quad (11)$$
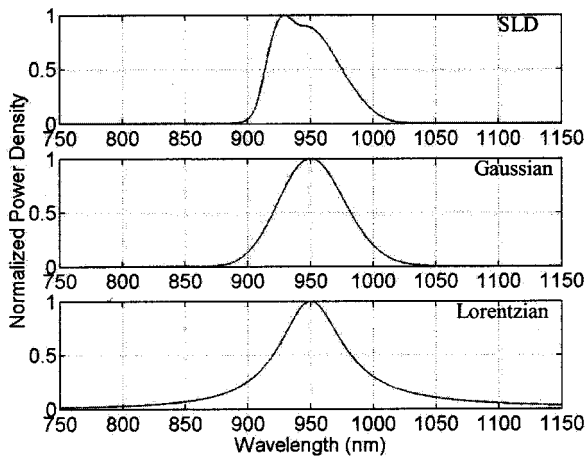
The coherence lengths of the source become

$$l_{c_{\text{FWHM}}} = \frac{2\ln(2)}{\pi}\frac{\lambda_0^{\,2}}{\Delta\lambda}. \quad (12)$$

$$l_c = \frac{\lambda_0^{\,2}}{\pi\Delta\lambda}. \quad (13)$$

The real light source we considered is a SLD (Superlum SLD-471). It is a broadband, low-coherence source centered at 950 nm with a -3-dB spectral bandwidth of 62 nm. In Fig. 2(a) we present the PSD of the real source, as well as the normalized Gaussian and Lorentzian PSDs given by Eqs. (6) and (10), where the center wavelength and bandwidth were set to match that of the SLD-471. The presented PSDs are normalized to unity for comparison. Figure 2(b) shows the computed modulus of the complex temporal coherence functions $|\gamma(\tau)|$ associated to each PSD in Fig. 2(a).

The spectrum analyzer, which is employed to measure the PSD of the SLD, provides a discrete data set of 1001 samples (N) with 0.4-nm resolution ($\delta\lambda$). The domain of the time delay τ depends on the center wavelength λ_0 and $\delta\lambda$ as $[-\lambda_0^{\,2}/(2c\delta\lambda), \lambda_0^{\,2}/(2c\delta\lambda)]$, such that the time-delay resolution $\delta\tau$ will be $\lambda_0^{\,2}/[(N-1)c\delta\lambda]$, which equals 7.513 fs. The complex temporal coherence function is estimated with an inverse fast Fourier transform.

Table 1 presents the computed coherence lengths of the SLD-471 and the two theoretical sources. As shown in Table 1, different spectral shapes present different coherence lengths, thus longitudinal resolutions for an optical coherence image, although they have the same bandwidth and center wavelength. Approximating the PSD of the SLD to a Gaussian function results in an error of approximately 10% for coherence lengths evaluated through both of the metrics. The results show that the coherence lengths computed from the Lorentzian PSD are approxi-

(a)
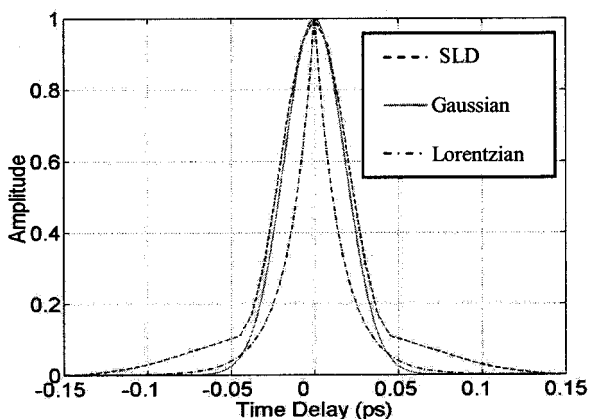
(b)

Fig. 2. (a) Measured PSD of the SLD: the normalized Gaussian PSD and the normalized Lorentzian PSD ($\lambda_0 = 950$ nm, $\Delta\lambda = 62$ nm for each). (b) Modulus of the corresponding complex degree of temporal coherence functions.

mately half of that of the coherence lengths of the Gaussian PSD and the SLD.

B. Computation of Coherence Lengths of Sources with Extended Power Spectral Densities

PSDs of real sources usually include spectral bumps and dips in their shapes, which lead to sidelobes in the interferometric signal. The sidelobes may significantly affect the resolution of the system. However, longitudinal resolution can always be estimated

Table 1. Coherence Length of Sources with Different-Shaped PSDs[a]

Source	$l_{c_{FWHM}}$ (μm)	l_c (μm)
SLD-471	14.14	10.78
Normalized Gaussian PSD	12.83	9.65
Normalized Lorentzian PSD	6.42	4.64

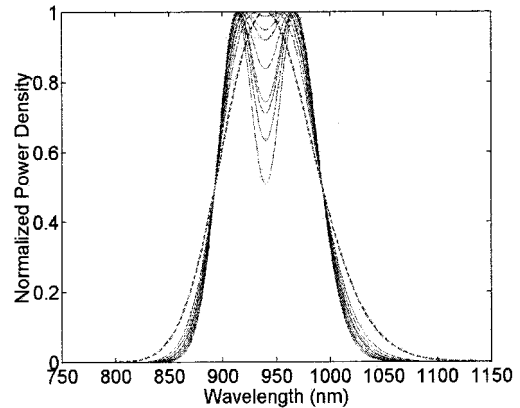[a]As presented in Fig. 2(a), computed according to two metrics.

Fig. 3. Gaussian PSD with a 100-nm −3-dB bandwidth centered at 940 nm (dashed curve) and PSDs of the same bandwidth and center wavelength with different spectral dip amplitudes.

from the measured PSD of the light source following the same metrics presented here.

The deformation (i.e., dips) of spectral shape of sources employed in optical coherence imaging is usually observed for high-power ($\sim 10^1$ to $\sim 10^2$ mW) broadband sources ($\sim 10^2$ nm), such as the Superlum SLD-47-HP with a Gaussian dip in its spectrum as shown in the specification sheet of the product, mode-locked Ti:Al$_2$O$_3$ laser source with multiple dips and bumps in its spectrum[10,15] and the SLD-370 as presented in a partial coherence interferometry experiment.[9]

We investigated the effect of a dip in the PSD of virtual sources on coherence lengths and associated longitudinal resolution. A Gaussian PSD with 100-nm −3-dB bandwidth centered at 940 nm was generated. We introduced spectral dips into the Gaussian PSD by subtracting Gaussian functions of a −3-dB 45-nm bandwidth centered at 940 nm of different magnitudes. Each resulting normalized PSD has a −3-dB 100-nm bandwidth with different levels of spectral dip. Figure 3 shows the Gaussian PSD (dashed curve) and the generated PSDs with spectral dips.

Power spectral analyses of these PSDs were performed. Figure 4 presents the plot of the numerical results for the coherence length of each PSD as a function of the percentage of the level difference between the dip minimum and the peaks of the PSD, where a zero percentage of the spectral dip refers to the Gaussian PSD. In Fig. 5 the simulated modulus of the temporal coherence functions of the PSDs with 49.13%, 5.1%, and no spectral dips is presented as examples. For all the Gaussian with dips, we estimated the coherence length using Eqs. (2) and (3). To validate the accuracy of these computations, we compared the values for the coherence length of the Gaussian with no dips obtained from Eqs. (2) and (3) with those obtained using Eqs. (8) and (9). Numerical computational errors of 0.3% and 0.8% were computed for the FWHM metric and the other metric, respectively. These numerical errors, which occur because of the discrete form of the PSD and
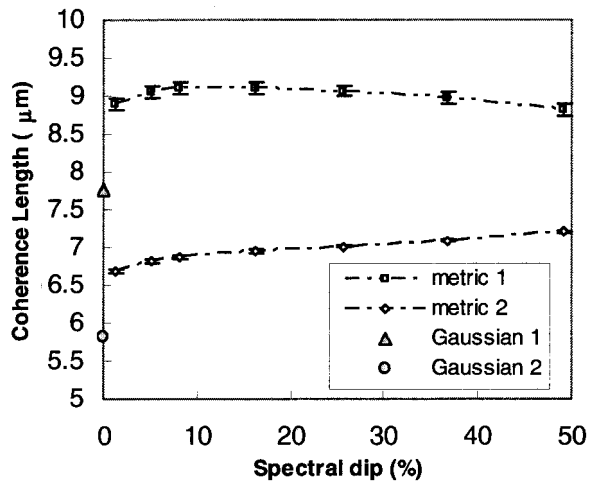
Fig. 4. Computed coherence length is presented as a function of the amplitude percentage of the spectral dip with metric 1 (FWHM criterion) and metric 2 (from integration). The circle and the triangle on the vertical axis represent, respectively, the coherence length of the Gaussian PSD, where Gaussian 1 corresponds to the FWHM and Gaussian 2 corresponds to the integration.

the temporal coherence functions, are small enough to neglect.

C. Ability to Resolve Two Layers

We predict here the ability to resolve two layers separated by Δz for selected sources presented in this paper. Referring to Fig. 1, we assume as detailed above that the phases of the complex temporal coherence functions are the same, and the index of refraction n' is chosen such that α, given by relation (5), equals one. We set the separation of these layers Δz to half of $l_{c_{\mathrm{FWHM}}}$ given by Eq. (2) and half of l_c given by Eq. (3), both presented in Table 1 and Fig. 4. We first considered the normalized Gaussian, Lorentzian, and SLD-471 PSDs, which were described in Subsection 3.A. The ability to resolve two layers is presented in Figs. 6(a)–6(c), respectively. Then we
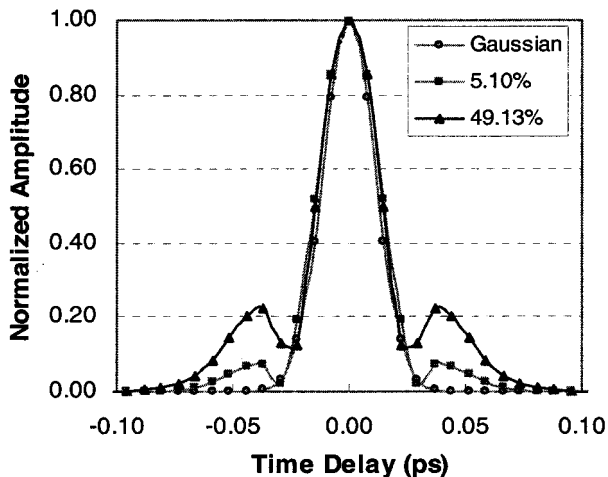

Fig. 5. $|\gamma(\tau)|$ of the PSDs of the 100-nm bandwidth centered at a 940-nm source with a selected percentage of spectral dip.

employed two of the PSDs, specifically with the 8.04% and the 49.13% spectral dips, presented in Subsection 3.B. The results are presented in Figs. 6(d) and 6(e).

4. Discussion

Significant differences in computed longitudinal resolution and coherence length for real and theoretical sources with the same bandwidth and center wavelength but with different spectral functions were presented. Such results demonstrate that it is important to take into account the shape of the source PSD in predicting resolution. A source with a slightly narrower spectral bandwidth than another source could possibly lead to higher resolution than the latter, simply based on its superior shape. Such findings are further strengthened by the analysis of coherence lengths from PSDs of the same spectral width, yet having varying amplitudes of spectral dips. Results show that, when a PSD with a spectral dip is approximated to a Gaussian PSD of the same center wavelength and bandwidth, it leads to incorrect values of coherence length obtained with either of the metrics considered.

A spectral dip in a PSD introduces sidelobes in the temporal coherence function. When computing the coherence length through the first metric, we measure the FWHM of the mainlobe disregarding the sidelobes. If the sidelobes are located close to the mainlobe, the overall FWHM of the temporal coherence function could be larger than the FWHM of the mainlobe. When we use the second metric to compute the coherence length, the integration process extends through the mainlobe and the sidelobes (e.g., Fig. 5). Integrating the sidelobes will result in a larger value of the coherence length and thus worse longitudinal resolution. However, if the sidelobes are far from the mainlobe, the effect on image quality will be ghost images, rather than a decrease in resolution.

In the simulations conducted on the basis of the separation of two layers and various PSDs, results show that two layers, with a separation of half of the FWHM of the modulus of the temporal coherence function, cannot always be resolved depending on the shape of the PSD of the source, as shown in Fig. 6(d). Also, the half of the coherence length derived through the integration does not provide a detectable separation of the layers except in the case of a source with Lorentzian PSD. Moreover, the plots in Fig. 6 indicate that the center of the resulting signal is not as low as 73.5% of the amplitude of the peak, which is required by the Rayleigh criterion for resolution. For the simulations that we carried out, it may be worthwhile to change the distance between the layers to the point where the signals can be separated according to the Rayleigh criterion.

The simulations presented in this paper will be limited in their ability to precisely predict experimental results. The first one is the phase mismatch discussed in Subsection 2.B, which could lead to a higher resolution than predicted. The second is the refrac-
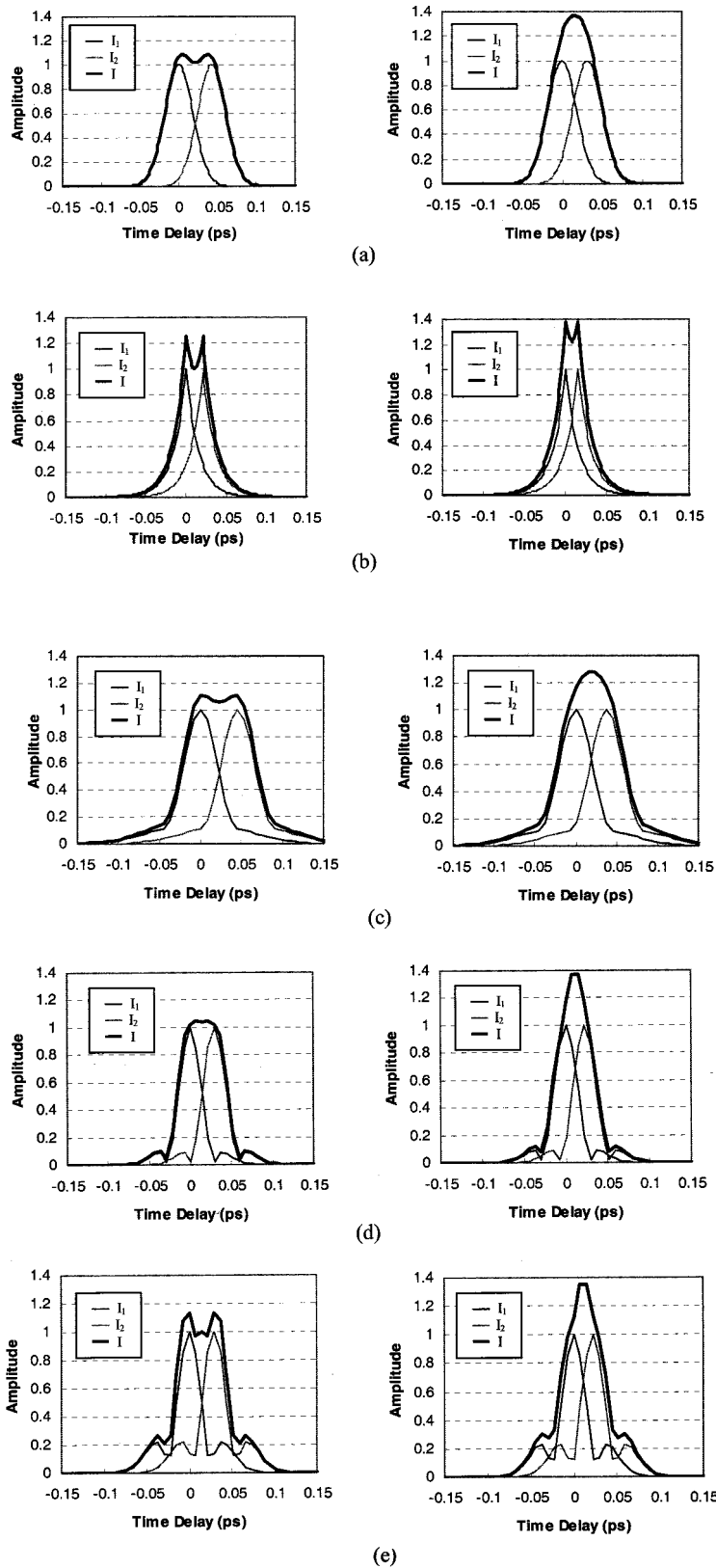
Fig. 6. Envelopes of the interferometric signals I_1 and I_2 that are due to backreflections from two successive layers (left column, $\Delta z = l_{c_{\mathrm{FWHM}}}/2$; right column, $\Delta z = l_c/2$) and the resulting signal I for a source with (a) Gaussian PSD, (b) Lorentzian PSD, (c) SLD-471 presented in Fig. 2(a), (d) PSD with 8.04% spectral dip amplitude, (e) PSD with 49.13% spectral dip amplitude presented in Fig. 3.

tive index n, which has to be taken into account in the resolution prediction, given that the media could affect significantly the resolution by dispersive and multiscattering effects. Finally, the setup, including the detection scheme, is also a source of decrease in resolution, given the group-velocity dispersion in the fiber, polarization mismatch between the two arms, unsuitable coating for the optical elements across the entire spectrum of the source, and noise. However, because an optimized setup can show good agreement between the self-coherence function derived from the PSD and the PSF measurement,[8–10] researchers can hope to overcome these experimental constraints.

Two additional remarks are necessary to end the discussion. The first one concerns the other aspects of the sources that are also important for the quality of optical coherence imaging, such as the dynamic range[16] and the temporal fluctuations.[15] The second one underscores the fact that the longitudinal resolution we have set is not the last limit we could achieve if we take into account image processing. Indeed, knowing the self-coherence function, the noise, and some optical properties of the media, an appropriate deconvolution operation may lead to improved longitudinal resolution.[17,18] Future researches will investigate such aspects.

5. Conclusion

A main purpose of this paper was to show that the shape of the spectrum of a source has a tremendous impact on the longitudinal resolution in optical coherence imaging and that the commonly made assumption of Gaussian-shaped PSDs may not provide an accurate prediction. A second purpose was to find a most appropriate metric to predict resolution from coherence length. Results show that neither of the metrics used in this paper is reliable to predict resolution as defined in Subsection 2.B for all cases of spectrum shapes. An upper bound on resolution, however, is best computed by means of finding the temporal separation between two delayed complex temporal coherence functions that leads to a fixed value in the center of the composed function, e.g., as defined in Rayleigh resolution criterion, obtained by a sum of the two delayed functions.

References

1. D. Huang, E. A. Swanson, C. P. Lin, J. S. Schuman, W. G. Stinson, W. Chang, M. R. Hee, T. Flotte, K. Gregory, C. A. Puliafito, and J. G. Fujimoto, "Optical coherence tomography," Science **254**, 1178–1181 (1991).
2. J. M. Schmitt, "Optical coherence tomography (OCT): a review," IEEE J. Sel. Top. Quantum Electron. **5**, 1205–1215 (1999).
3. A. F. Fercher, "Optical coherence tomography," J. Biomed. Opt. **1**, 157–173 (1996).
4. J. A. Izatt, M. D. Kulkarni, H. Wang, K. Kobayashi, and M. V. Sivak, Jr., "Optical coherence tomography and microscopy in gastrointestinal tissue," IEEE J. Sel. Top. Quantum Electron. **2,** 1017–1028 (1996).
5. J. K. Barton, A. J. Welch, and J. A. Izatt, "Investigating pulsed dye laser-blood vessel interaction with color Doppler optical coherence tomography," Opt. Express **3,** 251–256 (1998); http://www.opticsexpress.org.
6. J. W. Goodman, *Statistical Optics* (Wiley, New York, 1985), Chaps. 5 and 7.
7. R. Bracewell, *The Fourier Transform and Its Applications* (McGraw-Hill, New York, 1965), Chap. 8.
8. R. K. Wang, "Resolution improved optical coherence-gated tomography for imaging through biological tissues," J. Mod. Opt. **46,** 1905–1912 (1999).
9. C. K. Hitzenberger, A. Baumgartner, W. Drexler, and A. F. Fercher, "Dispersion effects in partial coherence interferometry: implications for intraocular ranging," J. Biomed. Opt. **4**, 144–151 (1999).
10. B. Bouma, G. J. Tearney, S. A. Boppart, M. R. Hee, M. E. Brezinski, and J. G. Fujimoto, "High-resolution optical coherence tomographic imaging using a mode-locked Ti:Al_2O_3 laser source," Opt. Lett. **20**, 1486–1488 (1995).
11. R. E. Ziemer and W. H. Tranter, *Principles of Communications* (Wiley, New York, 1995), Chap. 2.
12. L. Mandel and E. Wolf, *Optical Coherence and Quantum Optics* (Cambridge U. Press, New York, 1995), Chap. 4.
13. Y. Zhang, M. Sato, and N. Tanno, "Numerical investigations of optimal synthesis of several low coherence source for resolution improvement," Opt. Commun. **192**, 183–192 (2001).
14. Y. Pan, R. Birngruber, J. Rosperich, and R. Engelhardt, "Low-coherence optical tomography in turbid tissue: theoretical analysis," Appl. Opt. **34**, 6564–6575 (1995).
15. W. Drexler, U. Morgner, F. X. Kärtner, C. Pitris, S. A. Boppart, X. D. Li, E. P. Ippen, and J. G. Fujimoto, "*In vivo* ultrahigh-resolution optical coherence tomography," Opt. Lett. **24**, 1486–1488 (1999).
16. S. R. Chinn and E. A. Swanson, "Blindness limitations in optical coherence domain reflectometry," Electron. Lett. **29,** 2025–2027 (1993).
17. J. M. Schmitt, "Restoration of optical coherence images of living tissue using the clean algorithm," J. Biomed. Opt. **3**, 66–75 (1998).
18. M. D. Kulkarni, C. W. Thomas, and J. A. Izatt, "Image enhancement in optical coherence tomography using deconvolution," Electron. Lett. **33,** 1365–1367 (1997).